

1 **Ice formation on lake surface in winter causes warm season bias of lacustrine**
2 **brGDGT temperature estimates**

3
4 Jiantao Cao ^{1,2}, Zhiguo Rao ^{3,*}, Fuxi Shi ⁴, Guodong Jia ^{1,*}

5
6 ¹ State Key Laboratory of Marine Geology, Tongji University, Shanghai 200092, China

7 ² Key Laboratory of Western China's Environmental Systems, Ministry of Education, College of Earth
8 and Environmental Sciences, Lanzhou University, Lanzhou, 730000, China

9 ³ College of Resources and Environmental Sciences, Hunan Normal University, Changsha, 410081,
10 China

11 ⁴ Jiangxi Provincial Key Laboratory of Silviculture, College of Forestry, Jiangxi Agricultural
12 University, Nanchang, 330045, China

13 **Corresponding authors: Zhiguo Rao (raozhg@hunnu.edu.cn); Guodong Jia (jiagd@tongji.edu.cn).*

14

15 **Abstract**

16 It has been frequently found that lacustrine brGDGT-derived temperatures are warm season biased
17 relative to measured mean annual air temperature (AT) in the mid to high latitudes, the mechanism of
18 which, however, is not very clear. Here, we investigated the brGDGTs from catchment soils,
19 suspended particulate matter (SPM) and surface sediments in different water depths in the Gonghai
20 Lake in north China to explore this question. Our results showed that the brGDGT distribution in
21 sediments resembled that in the SPM but differed from the surrounding soils, suggesting a substantial
22 aquatic origin of the brGDGTs in the lake. Moreover, the increase of brGDGT content and decrease of
23 methylation index with water depth in sediments suggested more contribution of aquatic brGDGTs
24 produced from deep/bottom waters. Therefore, established lake-specific calibrations were applied to
25 estimate local mean annual AT. As usual, the estimates were significantly higher than the measured
26 mean annual AT. However, they were similar to, and thus actually reflected, the mean annual lake
27 water temperature (LWT). Interestingly, the mean annual LWT is close to the measured mean warm
28 season AT, hence suggesting that the apparent warm season bias of lacustrine brGDGT-derived
29 temperatures could be caused by the discrepancy between AT and LWT. In our study region, ice forms
30 at the lake surface during winter, leading to isolation of the underlying lake water from air and hence
31 higher LWT than AT, while LWT basically follows AT during warm seasons when ice disappears.
32 Therefore, we think what lacustrine brGDGTs actually reflected is the mean annual LWT, which is

33 higher than the mean annual AT in our study location. Since the decoupling between LWT and AT in
34 winter due to ice formation is a universal physical phenomenon in the mid to high latitudes, we
35 propose this phenomenon could be also the reason for the widely observed warm season bias of
36 brGDGT-derived temperatures in other seasonally surface ice-forming lakes, especially the shallow
37 lakes.

38 **Keywords:** lake sediments, aquatic brGDGTs, temperature proxy, seasonality, ice formation

39

40 **1 Introduction**

41 The branched glycerol dialkyl glycerol tetraethers (brGDGTs), including 0–2 cyclopentyl
42 moieties (a–c) and four to six methyl groups (I–III) (Weijers et al., 2007a), are components of the cell
43 membranes of microorganisms ubiquitously found in marine and continental environments and
44 sensitive to ambient environmental conditions (Sinninghe Damsté et al., 2000; Weijers et al., 2006a;
45 Schouten et al., 2013). The relative amounts of methyl groups and cyclopentyl moieties, expressed as
46 methylation index and cyclization ratio of brGDGTs (such as MBT/CBT or MBT'/CBT) in soil
47 brGDGTs, have been proposed to reflect mean annual air temperature (AT) (Weijers et al., 2007a;
48 Peterse et al., 2012). With improved analytical methods, a series of 6-methyl brGDGTs, previously
49 co-eluted with 5-methyl brGDGTs, were identified (De Jonge et al., 2013), which may introduce
50 scatter in the original MBT'/CBT calibration for the mean annual AT (De Jonge et al., 2014). Thus,

51 exclusion of the 6-methyl brGDGTs from the MBT', i.e. the newly defined MBT'_{5ME}, results in
52 improved calibrations (De Jonge et al., 2014; Wang et al., 2016; Wang et al., 2019). Calibrations using
53 globally distributed surface soils for the MBT/CBT, MBT'/CBT or MBT'_{5ME} indices (Weijers et al.,
54 2007a; Peterse et al., 2012; De Jonge et al., 2014) have been widely used for continental AT
55 reconstruction (e.g., Weijers et al., 2007b; Niemann et al., 2012; Lu et al., 2019).

56 BrGDGTs in lake environments were initially thought to be derived from soil input (Hopmans et
57 al., 2004; Blaga et al., 2009), allowing the mean annual AT to be reconstructed from lake sediments.
58 However, when the soil-based calibrations are applied to the lake materials, the estimated
59 temperatures are usually significantly lower than actual local AT (Tierney and Russell, 2009; Tierney
60 et al., 2010; Blaga et al., 2010; Loomis et al., 2011, 2012; Pearson et al., 2011; Sun et al., 2011;
61 Russell et al., 2018), suggesting an intricate brGDGT response to ambient temperature in aquatic
62 environments. Later, more and more studies reveal that brGDGTs could be produced in situ in lake
63 environments and differ significantly from soil derived brGDGT distributions (Wang et al., 2012;
64 Loomis et al., 2014; Naeher et al., 2014; Hu et al., 2015; Cao et al., 2017) and stable carbon isotope
65 composition (Weber et al., 2015, 2018). The findings of intact polar lipid of brGDGTs, indicative of
66 fresh microbial products, in lake water suspended particulate matter (SPM) and surface sediments
67 (Tierney et al., 2012; Schoon et al., 2013; Buckles et al., 2014a; Qian et al., 2019) further confirm the
68 in-situ production of brGDGTs. Nevertheless, the brGDGT distribution in lake surface sediments has

69 been found to be still strongly correlated with AT. Subsequently, quantitative lacustrine-specific
70 calibrations for AT have been established at regional and global scales (Tierney et al., 2010; Pearson
71 et al., 2011; Sun et al., 2011; Loomis et al., 2012; Shanahan et al., 2013; Foster et al., 2016; Dang et
72 al., 2018; Russell et al., 2018), which have been widely used for AT reconstruction. These
73 lacustrine-specific calibrations may reflect mean annual AT well in low-latitude regions (Tierney et al.,
74 2010; Loomis et al., 2012), such as in the Lake Huguangyan (21°09' N, 110°17' E) in south China (Hu
75 et al., 2015), Lake Donghu (30°54' N, 114°41' E) in central China (Qian et al., 2019) and Lake Towuli
76 (2°30' S, 121° E) on the island of Sulawesi (Tierney and Russell, 2009). However, they usually yield
77 estimates biased to the warm/summer seasons in mid- and high-latitude regions (Shanahan et al., 2013;
78 Foster et al., 2016; Dang et al., 2018), such as in Lake Qinghai (36°54' N, 100°01' E) in the
79 northeastern Tibetan Plateau (Wang et al., 2012), in Lower King Pond (44°25' N, 72°26' W) in
80 temperate northern Vermont, U.S.A. (Loomis et al., 2014) and in the Arctic lakes (Peterse et al., 2014).
81 The warm biased temperature estimates in the mid- and high-latitude lakes have been postulated to be
82 caused by the higher brGDGT production during warm seasons (e.g., Pearson et al., 2011; Shanahan
83 et al., 2013).

84 BrGDGT-producing bacteria in soils could be metabolically active, hence producing abundant
85 brGDGTs in warm and humid season, but suppressed in cold and/or dry environments (Deng et al.,
86 2016; De Jonge et al., 2014; Naafs et al., 2017). However, it is presently unclear whether the

87 brGDGTs in lacustrine sediments are mainly produced during the warm season. Investigations on lake
88 water SPM reveal higher concentration of brGDGTs in the water column may occur in different
89 seasons, e.g., in winter in Lake Lucerne in central Switzerland (Blaga et al., 2011), Lake Challa in
90 tropical Africa (Buckles et al., 2014a) and Lake Huguangyan in subtropical southern China (Hu et al.,
91 2016), in spring and autumn in Lower King Pond in temperate northern Vermont, U.S.A. (Loomis et
92 al., 2014), and in warm season in Lake Donghu in central China (Qian et al., 2019). Moreover, the
93 contribution of the aquatic brGDGTs to the sediments is quantitatively unknown, and likely minor
94 considering that brGDGT producers favor anoxic conditions (Weijers et al., 2006b; Weber et al., 2018)
95 that usually prevail in bottom water and sediments, which may discount the application of
96 SPM-derived findings to the sedimentary brGDGTs.

97 In fact, brGDGT-based temperature indices should directly record lake water temperature (LWT),
98 rather than AT, if the brGDGTs in lake sediments solely or mainly sourced from the lake environments
99 (Tierney et al., 2010; Loomis et al., 2014). So, the mean annual AT estimate based on lake
100 sedimentary brGDGTs is valid only when LWT is tightly coupled with AT. However, the relationship
101 between LWT and AT is potentially complex in cold regions, as well as in deep lakes, and the
102 coupling between the two is not always the case, which would hamper the application of brGDGTs for
103 temperature estimates (Pearson et al., 2011; Loomis et al., 2014; Weber et al., 2018). In deep lakes,
104 bottom water temperature usually decouples with AT, together with the predominant production of

105 brGDGTs in deep water and sediments, causing weak correlations between brGDGT-derived
106 temperature and AT (Weber et al., 2018). For shallow lakes, LWT does not always follow AT either,
107 specifically in winter when AT is below the freezing point in cold regions, as has been shown in the
108 Lower King Pond (Loomis et al., 2014). However, the decoupling between LWT and AT has not been
109 recognized as a key mechanism for the warm bias of brGDGT-derived temperatures observed widely
110 in the mid- and high-latitude lakes, and seasonal production or deposition of brGDGTs is usually
111 invoked as a cause (e.g., Pearson et al., 2011; Shanahan et al., 2013; Loomis et al., 2014). Here, we
112 hypothesized that the decoupling between LWT and AT in mid- and high-latitude shallow lakes, rather
113 than the warm season production, could have caused the frequently observed warmer temperature
114 estimates from the lacustrine brGDGTs. To test this hypothesis, we investigated the Gonghai Lake (a
115 shallow alpine lake) in north China by collecting SPM and surface sediments in different depths in the
116 lake and soils in its catchment in a hot summer and a cold winter. We analyzed brGDGT distributions
117 in these materials to determine the sources of brGDGTs in the lake and further discussed the possible
118 reasons for the warm bias of brGDGT-estimated temperatures.

119

120 **2 Materials and methods**

121 **2.1 Gonghai Lake**

122 The Gonghai Lake [38°54' N, 112°14' E, ca. 1860 m above sea level (a.s.l.); Fig. 1a and 1b] is

123 located on a planation surface of the watershed between the Sang-kan River and the Fenhe River at
124 the northeast margin of the Chinese Loess Plateau. The location is close to the northern boundary of
125 the modern East Asian summer monsoon (EASM, Chen et al., 2008; Fig. 1a). The modern local
126 climate is controlled mainly by the East Asian monsoon system, with a relatively warm and humid
127 summer resulting from the prevailing EASM from the southeast, and a relatively cold and arid winter
128 under the prevailing East Asian winter monsoon (EAWM) from the northwest (Chen et al., 2013,
129 2015; Rao et al., 2016). The mean annual precipitation is ca. 482 mm, concentrated (75%) between
130 July and September (Chen et al., 2013). Its total surface area is ca. 0.36 km² and the maximum water
131 depth is ca. 10 m. Based on a nearby weather station, the measured mean annual AT is 4.3 °C for the
132 past 30 years. The warm season lasts from May to September (Fig. 1c), when column stratification
133 develops with an upper-bottom temperature difference >1 °C. During the winter from November to
134 March, ice forms on the lake surface, and LWT under ice vertically constant at ca. 4 °C, which is
135 significantly higher than AT that is much below the freezing point (Fig. 1c). From April to October,
136 the ice disappears and LWT follows AT closely, demonstrating a coupling between them (Fig. 1c).
137 The vegetation type of the planation surface belongs to transitional forest-steppe, dominated by *Larix*
138 *principis-rupprechtii*, *Pinus tabulaeformis* and *Populus davidiana* forest, *Hippophae rhamnoides*
139 scrub, *Bothriochloa ischaemum* grassland and *Carex spp.* (Chen et al., 2013; Shen et al., 2018).

140 **2.2 Sampling**

141 In September 2017, five surface soil samples in the catchment and five surface sediment samples
142 at different depths (1.0, 2.5, 5.5, 6.7 and 8.0 m) in Gonghai Lake were collected (Fig. 1b). At each soil
143 sample site, we collected 5–6 subsamples (top 0–2 cm) within an area of ca. 100 m² with contrasting
144 micro-topography or plant cover and then mixed them to represent a single sample. To avoid possible
145 human disturbances, the soil sampling sites were distant from roads and buildings. All samples
146 collected in the field were stored in a refrigeration container during transportation and then
147 freeze-dried for >48 h in the laboratory. Details of all the sampling sites, including locations, sample
148 depth and vegetation type, are listed in Table 1.

149 In addition, we also collected two batches of SPM samples at water depth of 1 m, 3 m, 6 m and 8
150 m by filtering 50 L water through a 0.7 µm Whatman GF/F filter on site in September 2017 and
151 January 2018, respectively. SPM samples were also stored in a refrigeration container during
152 transportation and then freeze-dried for >48 h in the laboratory. At the same time of SPM sampling,
153 we measured water column parameters in the lake using an YSI water quality profiler.

154 **2.3 Sample treatment and GDGT analysis**

155 Freeze-dried soil and sediment samples were homogenized at room temperature and accurately
156 weighed. Each freeze-dried filter with SPM attached was cut into small pieces using a sterilized
157 scissor. Each sample of soil, sediment and SPM was placed in a 50 ml tube and then ultra-sonicated
158 successively with dichloromethane/methanol (DCM/MeOH, 1:1, v/v) four times. After centrifugation

159 and combination of all the extracts of a sample, an internal standard, synthesized C₄₆ GDGT, was
160 added with a known amount (Huguet et al., 2006). Subsequently, the total extracts were concentrated
161 using a vacuum rotary evaporator. The nonpolar and polar fractions in the extracts were separated via
162 silica gel column chromatography, using pure *n*-hexane and DCM/MeOH (1:1, v/v), respectively. The
163 polar fraction containing GDGTs was dried in a gentle flow of N₂, dissolved in *n*-hexane/ethyl acetate
164 (EtOA) (84:16, v/v) and filtered through a 0.45 µm polytetrafluoroethylene filter before instrumental
165 analysis. We performed GDGT analysis by high performance liquid chromatography-atmospheric
166 pressure chemical ionization-mass spectrometry (HPLC-APCI-MS; Agilent 1200 series 6460 QQQ).
167 Following the method of Yang et al. (2015), the separation of 5- and 6-methyl brGDGTs was achieved
168 using two silica columns in tandem (150 mm × 2.1 mm, 1.9 µm, Thermo Finnigan; U.S.A.)
169 maintained at 40 °C. The following elution gradient was used: 84/16 *n*-hexane/EtOA (A/B) to 82/18
170 A/B from 5 to 65 min and then to 100% B in 21 min, followed by 100% B for 4 min to wash the
171 column and then back to 84/16 A/B to equilibrate it for 30 min. The flow rate was at a constant 0.2
172 ml/min throughout. BrGDGTs were ionized and detected with single ion monitoring (SIM) at *m/z*
173 1050, 1048, 1046, 1036, 1034, 1032, 1022, 1020, 1018 and 744. The brGDGTs were quantified by
174 comparing peak area of each brGDGT compound with the C₄₆ GDGT internal standard. Based on
175 duplicate HPLC/MS analyses, the analytical errors of both the MBT'_{5ME} and MBT'_{6ME} index were
176 ±0.01 units.

177 2.4 Calculation of GDGT-related Proxies

178 The MBT'_{5ME} and MBT'_{6ME} index were calculated following Eq. (1) and (2) as in De Jonge et al.
179 (2014):

$$180 \text{MBT}'_{5\text{ME}} = (\text{Ia}+\text{Ib}+\text{Ic}) / (\text{Ia}+\text{Ib}+\text{Ic}+\text{IIa}+\text{IIb}+\text{IIc}+\text{IIIa}) \quad (1)$$

$$181 \text{MBT}'_{6\text{ME}} = (\text{Ia}+\text{Ib}+\text{Ic}) / (\text{Ia}+\text{Ib}+\text{Ic}+\text{IIa}'+\text{IIb}'+\text{IIc}'+\text{IIIa}') \quad (2)$$

182 The isomer ratio (IR) of 6-methyl was calculated as in De Jonge et al. (2014). The $\Sigma\text{IIIa}/\Sigma\text{IIa}$ ratio was
183 calculated as in Martin et al. (2019), which is modified from Xiao et al. (2016). The weighted average
184 number of ring moieties ($\#\text{Rings}_{\text{tetra}}$, $\#\text{Rings}_{\text{penta } 5\text{ME}}$ and $\#\text{Rings}_{\text{penta } 6\text{ME}}$) followed Sinnighe Damsté
185 (2016):

$$186 \text{IR}_{6\text{ME}} = (\text{IIa}'+\text{IIb}'+\text{IIc}'+\text{IIIa}'+\text{IIIb}'+\text{IIIc}') / (\text{IIa}+\text{IIa}'+\text{IIb}+\text{IIb}'+\text{IIc}+\text{IIc}'+\text{IIIa}+\text{IIIa}'+\text{IIIb}+\text{IIIb}'+\text{IIIc}+\text{IIIc}') \quad (3)$$

$$188 \Sigma\text{IIIa}/\Sigma\text{IIa} = (\text{IIIa}+\text{IIIa}'+\text{IIIa}'') / (\text{IIa}+\text{IIa}') \quad (4)$$

$$189 \#\text{Rings}_{\text{tetra}} = (\text{Ic} * 2 + \text{Ib}) / (\text{Ia} + \text{Ib} + \text{Ic}) \quad (5)$$

$$190 \#\text{Rings}_{\text{penta } 5\text{ME}} = (\text{IIc} * 2 + \text{IIb}) / (\text{IIa} + \text{IIb} + \text{IIc}) \quad (6)$$

$$191 \#\text{Rings}_{\text{penta } 6\text{ME}} = (\text{IIc}' * 2 + \text{IIb}') / (\text{IIa}' + \text{IIb}' + \text{IIc}') \quad (7);$$

192 The Roman numerals represent different brGDGT homologues referred to Yang et al. (2015) and
193 Weber et al. (2015) (see Appendix 1).

194 In this study, we used two silica columns in tandem and successfully separated 5- and 6-methyl

195 brGDGTs. However, many previous brGDGT studies on lake materials used one cyano column,
196 which did not separate 5- and 6-methyl brGDGTs (e.g., Wang et al., 2012; Loomis et al., 2014; Hu et
197 al., 2015, 2016; Cao et al., 2017). In order to facilitate comparison with previous studies, we
198 reanalyzed the published brGDGT data without separation of 5- and 6-methyl brGDGTs in the
199 Gonghai Lake (Cao et al., 2017). For temperature estimations, we listed the Eqs. (8–17) used in this
200 study in Table 2.

201

202 **3 Results**

203 **3.1 Seasonal changes in environmental parameters**

204 The AT in our study area ranged from -12.2 to 21.6 °C, below the freezing point in winter
205 (November to February) and at 4.3 °C for the mean in the year 2018 (Fig. 1c). Surface LWT ranged
206 from 3.4 to 21.9 °C (average 10.6 °C), and remained stable at ca. 4 °C in winter (Fig. 1c). In
207 September 2017, water column stratification was weak with temperature ranging from 16.9 to 17.8 °C
208 and exhibiting a gradual and slight decrease with depth (Fig. 2). In January 2018, the lake surface
209 water was frozen and LWTs under ice were 4 °C at all depths (Fig. 2).

210 **3.2 Concentration and distribution of brGDGTs**

211 BrGDGTs were detected in all samples, and their total concentration ranged between 16 – 75 ng/g
212 dry weight (dw) in surface soils from Gonghai catchment, 42 – 707 ng/g dw in lake surface sediments,

213 5–10 ng/l in September and 3–8 ng/l in January in water SPM (Table 1 and Fig. 2). The average
214 content of brGDGTs in lake surface sediments (291 ng/g dw) was significantly higher than in surface
215 soils (31 ng/g dw) and particularly exhibited an increasing trend with water depth. In SPM, the
216 average concentration of brGDGTs in water column showed no significant difference between
217 September and January ($t = 1.2$, $p = 0.26$) but there was a clearer trend of increase with depth in
218 September than in January (Fig. 2). Notably, the compound IIIa", which was regarded typical for in
219 situ produced lacustrine brGDGTs (Weber et al., 2015), was also identified in the Gonghai Lake
220 sediments and SPM but not found in catchment soils (Table 1 and Fig. 3a). There was no significant
221 difference in average concentration of IIIa" in water column between September and January ($t = 0.62$,
222 $p = 0.28$). The change patterns of IIIa" with water depth in SPM and sediments were the same as those
223 of the total brGDGTs (Table 1).

224 The brGDGTs in soils, sediments and SPM were dominated by brGDGT II and III series, with
225 acyclic compounds dominant in every series (Fig. 3a). In comparison, the mean $\Sigma\text{IIIa}/\Sigma\text{IIa}$ ratio value
226 in sediments (1.14–1.52 range, 1.30 average) was higher than in SPM (0.84–1.11 range, 0.99 average)
227 and soils (0.56–0.86 range, 0.70 average). In addition, 6-methyl brGDGTs dominated over 5-methyl
228 brGDGTs in soils, exhibiting mean $\text{IR}_{6\text{ME}}$ of 0.62; whereas the two isomers were similar in content in
229 sediments ($\text{IR}_{6\text{ME}} = 0.47\text{--}0.60$ range, 0.51 average) and SPM ($\text{IR}_{6\text{ME}} = 0.45\text{--}0.50$ range, 0.48 average)
230 (Fig. 3a).

231 **3.3 Cyclisation ratio and methylation index of brGDGTs**

232 The #Rings_{tetra} values varied from 0.26 to 0.45 (0.36 average) in catchment soils, 0.37–0.43 (0.40
233 average) in September and 0.39–0.42 (0.40 average) in January in SPM, and 0.45–0.47 (0.45 average)
234 in surface sediments (Fig. 3b). The #Rings_{penta 5ME} showed the same increasing trend as #Rings_{tetra}
235 from soils to SPM and then to sediments (Fig. 3b). In contrast, #Rings_{penta 6ME} in soils was similar to
236 that in sediments and SPM (Fig. 3b).

237 The MBT'_{5ME} values varied from 0.31 to 0.36 (0.35 average) in catchment soils, 0.23–0.29 (0.26
238 average) in surface sediments, 0.23–0.28 (0.26 average) in September and 0.24–0.26 (0.25 average) in
239 January in SPM (Fig. 3b). Generally, the MBT'_{5ME} exhibited decreasing trends with water depth in
240 surface sediments and SPM in September (Fig. 2). The MBT'_{6ME} values varied from 0.20 to 0.33 (0.25
241 average) in surface soils of the lake catchment, 0.22–0.27 (0.25 average) in surface sediments,
242 0.24–0.32 (0.28 average) in September and 0.26–0.28 (0.27 average) in January in SPM (Fig. 3b). The
243 MBT'_{6ME} also decreased in SPM in September, but increased in sediments with water depth. Both
244 MBT'_{5ME} and MBT'_{6ME} changed less in SPM in January with water depth (Fig. 2).

245

246 **4 Discussions**

247 **4.1 In situ production of brGDGTs in the Gonghai Lake**

248 Although brGDGTs have a strong potential to record temperature in lacustrine regions (Tierney

249 et al., 2010; Pearson et al., 2011; Sun et al., 2011; Loomis et al., 2012; Dang et al., 2018; Russell et al.,
250 2018), the sources of brGDGTs in lake sediments should be carefully identified. There are two
251 potential sources, including allochthonous input from soil and autochthonous production in lake water
252 and/or surface sediments, which can be distinguished by comparison of brGDGT distribution between
253 surface sediments and soils (Tierney and Russell, 2009; Loomis et al., 2011; Wang et al., 2012; Hu et
254 al., 2015; Sinninghe Damsté, 2016).

255 In the Gonghai Lake, the average content of brGDGTs in surface sediments was significantly
256 higher than that in surface soils (Table 1). Moreover, they exhibited a clearly increasing trend with
257 water depth, suggesting a possible autochthonous contribution, even though soil brGDGTs input
258 cannot be ignored. Moreover, the brGDGT distribution in surface sediments was similar to that of
259 SPM, but quite different from that of soils (Fig. 3a). Several lines of evidence indicate a substantial in
260 situ production of brGDGTs in the Gonghai Lake. (I) The presence of IIIa" in the Gonghai Lake
261 sediments and SPM but the absence in the catchment soils may be a direct evidence of in situ
262 production in the lake (Fig. 3a). A similar conclusion has been drawn in a Swiss mountain lake basin
263 (Weber et al., 2015). (II) In the Gonghai Lake, the $\Sigma\text{IIIa}/\Sigma\text{IIa}$ ratio in sediments (1.3 average) and
264 SPM (0.99 average) were much higher than in catchment soils (0.7 average) (Fig. 3a). The values of
265 $\Sigma\text{IIIa}/\Sigma\text{IIa} > 0.92$ has been regarded as the evidence of aquatic production in previous reports (Xiao et
266 al., 2016; Martin et al., 2019; Zhang et al., 2020). (III) The average values of $\text{IR}_{6\text{ME}}$ in surface

267 sediments and SPM were significantly lower than in catchment soils (Fig. 3a), suggesting at least
268 some of 5-methyl brGDGTs in lake sediments and SPM were produced in situ. (IV) The cyclisation
269 ratio of brGDGTs has been also used to distinguish the aquatic production from soil input, although
270 applied to marine sediments (Sinninghe Damsté, 2016). In the Gonghai Lake, #Rings_{tetra} and
271 #Rings_{penta 5ME} were clearly higher in sediments than in catchment soils ($p < 0.05$ for #Rings_{tetra}, p
272 < 0.01 for #Rings_{penta 5ME}), although #Rings_{penta 6ME} in sediments was similar to that in catchment soils
273 ($p = 0.11$ for #Rings_{penta 6ME}; Fig. 3b).

274 The in situ production of brGDGTs in the Gonghai Lake can be also evidenced by the
275 discrepancies in reconstructed temperatures between soils and sediments/SPM. Based on the new
276 global soil calibration of Eq. (9) and regional soil calibration of Eq. (10) for China, the
277 brGDGT-derived AT in the Gonghai catchment soils ranged from 1.18 to 2.75 °C (average $2.33 \pm$
278 0.65 °C; Table 1) and from -4.22 to -1.21 °C (average -2.42 ± 1.19 °C; Table 1), respectively.
279 Considering the ± 4.8 °C uncertainty of the global calibration and ± 2.5 °C of the regional calibration,
280 the estimated temperatures from the global calibration are much close to the mean annual AT of
281 4.3 °C, thereby well reflecting mean annual AT in our study lake catchment. Then, the global
282 calibration Eq. (9) was applied to sediment/SPM data, yielding estimated temperatures $-0.50 \pm$
283 0.78 °C in surface sediments and -0.55 ± 0.52 °C in SPM and hence much lower than those from
284 surface soils (2.33 ± 0.65 °C; Table 1). Similarly, temperature underestimation using soil-derived

285 calibration has been widely reported in many modern lake sediments (e.g., Tierney et al., 2010;
286 Loomis et al., 2012; Pearson et al., 2011; Russell et al., 2018), which has been attributed to in situ
287 production of brGDGTs in the lakes.

288 **4.2 Lacustrine brGDGT-derived ATs are warm season biased (average monthly** 289 **temperature >0 °C)**

290 The suggested in situ production of brGDGTs prompted us to use lake-specific temperature
291 calibrations (Tierney et al., 2010; Pearson et al., 2011; Sun et al., 2011; Loomis et al., 2012; Dang et
292 al., 2018; Russell et al., 2018) to reconstruct AT, although not differentiated quantitatively the relative
293 contributions of aquatic vs. soil-derived brGDGTs. Here, we applied four equations, Eqs. (11) and
294 (15)–(17) in Table 2, to our sedimentary brGDGT data.

295 As shown in Fig. 4a, the reconstructed temperatures using different equations are >6.4 °C.
296 Despite discrepancies in the temperature values between calibrations, they are comparable
297 considering the uncertainty of each calibration. A prominent feature of the reconstructed temperature
298 is that they, especially those in the shallower sediments, are well above the annual mean AT but more
299 close to the mean warm season AT (average monthly temperature >0 °C). This feature is consistent
300 with numerous studies proposing that lacustrine brGDGT-derived ATs are warm season biased
301 (Shanahan et al., 2013; Peterse et al., 2014; Dang et al., 2018).

302 Many previous brGDGT instrumental analyses on lake materials used one cyano column, which

303 did not separate 5- and 6-methyl brGDGTs. Using the data published in the same lake from Cao et al.
304 (2017), we re-calculated temperature using different calibrations. The results showed that the absolute
305 temperature estimates were all significantly warmer than the mean annual AT (Table 3), with the
306 temperature offsets varying from 4–10 °C, which cannot be fully explained by the uncertainty of each
307 calibration. Therefore, it appears that sedimentary brGDGT-derived temperature is warm season
308 biased in the Gonghai Lake irrespective of whether or not 5- and 6-methyl brGDGTs are separated.

309 Moreover, we found the warm season bias of reconstructed AT is increasingly apparent with the
310 increase of latitude. Here, five lakes, including Lower King Pond (Loomis et al., 2014), Qinghai Lake
311 (Wang et al., 2012), Lake Donghu (Qian et al., 2019), Huguangyan maar (Hu et al., 2015, 2016) and
312 Lake Towuli (Tierney and Russell, 2009), were selected to compare as an example. These lakes are
313 located in different regions spanning a relatively large environmental gradient, and more importantly,
314 brGDGT data from both the lake surface sediments and the surrounding soils are available. We
315 re-calculated temperatures from published data of brGDGTs from these lakes (Fig. 5) by applying the
316 calibration of global soils (Eq (8); Peterse et al., 2012) to the surrounding soils and the calibration of
317 lake surface sediments (Eq (11); Sun et al., 2011) to the lake sediments. As shown in Fig. 5a, the
318 brGDGT-inferred temperatures in catchment soils are similar to local mean annual ATs. In contrast,
319 the brGDGT-inferred temperatures in lake sediments are similar to the local mean annual ATs only in
320 low-latitude lakes, whereas they become increasingly higher than the local mean annual ATs toward

321 higher latitudes (Fig. 5b). In comparison, the brGDGT-inferred temperatures are close to the local
322 mean ATs in warm season (average monthly mean AT $>0^{\circ}\text{C}$) in all these lakes (Fig. 5c). Besides
323 above discussed lakes, some investigations have also pointed out that brGDGT-inferred temperatures
324 are higher than mean annual AT and close to warm season AT or summer AT in mid- and high-latitude
325 lakes (Shanahan et al., 2013; Peterse et al., 2014; Foster et al., 2016; Dang et al., 2018), whereas they
326 are close to, or lower than, mean annual AT in low-latitude lakes (Tierney et al., 2010; Loomis et al.,
327 2012). Therefore, it is a global occurrence that sedimentary brGDGT-derived temperatures are warm
328 season biased in lakes at cold regions.

329 4.3. Lacustrine brGDGTs reflect deep/bottom water temperature

330 Another feature of sedimentary brGDGT-derived ATs in our results is that there is a consistently
331 decreasing trend of reconstructed temperature with depth using Eqs. (11), (15) and (16) (Fig. 4a),
332 albeit less clear using Eq. (15). It is not understandable that AT is correlated with water depth.
333 Interestingly, both $\text{MBT}'_{5\text{ME}}$ and $\text{MBT}'_{6\text{ME}}$ in SPM showed decreasing trends with water depth in
334 September, similar to the water temperature profile of the month (Fig. 2). In January, the relatively
335 unchanged $\text{MBT}'_{5\text{ME}}$ and $\text{MBT}'_{6\text{ME}}$ (<0.02) also mirror the constant water temperature of the month
336 (Fig. 2). Accordingly, we surmise that brGDGT-derived temperatures in sediments and SPM may
337 actually reflect water temperature.

338 Although the $\text{MBT}'_{5\text{ME}}$ and $\text{MBT}'_{6\text{ME}}$ in SPM in the lake seem to reflect temperature changes in

339 the water column to some extent, the differences of brGDGT-derived temperatures based on
340 lake-specific calibrations between September and January (-0.93 to 1.21 °C) are much lower than the
341 measured difference (~ 13 °C), independent of the calibration of (15), (16) or (17) (Tables 1 and 2). In
342 fact, similar results have been also reported in other lakes. For example, in the Lower King Pond, the
343 calculated seasonal temperature difference in surface water SPM was 5.4 °C, significantly smaller
344 than the measured difference about 28.3 °C (Loomis et al., 2014); in the Lake Huguangyan, the
345 calculated seasonal temperature difference was 8 °C, also significantly smaller than the measured
346 difference about 16 °C (Hu et al., 2016). The reduced seasonal contrasts in SPM brGDGT-derived
347 temperatures could result from the existence of “fossil” brGDGTs and sediment resuspension in the
348 water column, which may lead to a long (e.g., multi seasonal) residence time of SPM, although not
349 exactly known (Loomis et al., 2014). The even smaller differences in MBT'_{5ME} and MBT'_{6ME} between
350 sediments and SPM at deeper sites in our results (Fig. 2) suggest the impacts of sediment suspension
351 on SPM. Such a scenario may lead to more “fossil” brGDGTs in SPM than those produced within a
352 specific season or month, as evidenced by an observation showing that only a small proportion of
353 intact polar lipid of brGDGTs, indicative of fresh brGDGTs, was detected in total brGDGTs in SPM
354 in a shallow lake (Qian et al., 2019). Besides, several parameters, such as $\Sigma IIIa/\Sigma IIa$, IR_{6ME} , $\#Rings_{tetra}$
355 and $\#Rings_{penta}$ in SPM, were in-between the soil and sediment values, we speculate terrestrial inputs
356 may be a factor, if any, to reduce the seasonal changes of brGDGTs in SPM.

357 In addition to reflecting water temperature, the decrease trend with depth in sedimentary
358 brGDGT-derived temperature further suggests a controlling influence of deep/bottom water
359 temperature. Similar occurrence has been observed also in Lower King Pond in temperate northern
360 Vermont, U.S.A. and Lake Biwa in central Japan, showing that the sedimentary brGDGT-derived
361 temperatures decreased with water depth, co-varied with mean annual LWT at depths (Ajiako et al.,
362 2014; Loomis et al., 2014). Also in Loch Lomond in the UK, the brGDGT-derived temperatures by
363 different MBT/CBT lacustrine calibrations all decreased with water depth (Buckles et al., 2014b). So,
364 a water depth-related production of brGDGTs should be considered when interpreting
365 brGDGT-derived temperatures, which will be discussed below.

366 A recent publication reported that changes in microbial community composition may be
367 responsible for variations in the distribution of brGDGTs, causing the different responses of soil
368 brGDGTs temperature, as well as pH, under different temperature ranges (De Jonge et al. 2019).
369 However, little is known about whether this idea is applicable to aquatic environments. According to
370 De Jonge et al. (2019), community change can be indicated by the community index ($CI = I_a / (I_a + I_b + I_c)$) in soils, with $CI > 0.64$ indicating warm community cluster and $CI < 0.64$ indicating cold
371 community cluster. Here we applied the CI to lake sediment data including ours and those available
372 for the entire 15 brGDGT compounds in literature, mostly from the east Africa. As shown in Fig. 4b,
373 the putative two community clusters also occur in lake environments, with the Gonghai community
374

375 belonging to the “cold” cluster. Different from soil data showing that MBT'_{5ME} captures large
376 temperature changes only when the bacterial community shows a strong change in composition (De
377 Jonge et al. 2019), it seems that MBT'_{5ME} changes linearly with LWT, which is less influenced by the
378 bacterial community change (Fig. 4b). However, we note that the test of community change here is
379 rather crude, and further studies on the biological sources of brGDGTs and their responses to
380 temperature in aquatic environments are needed.

381 **4.4 Ice cover formation as a mechanism for the apparent warm bias of lacustrine** 382 **brGDGT-derived temperature**

383 One explanation for the warm season biases of the lacustrine brGDGT-derived temperature in
384 mid to high latitudes has been proposed as the excessive production of brGDGTs during the
385 warm/summer season relative to winter season (Pearson et al., 2011; Shanahan et al., 2013; Peterse et
386 al., 2014; Foster et al., 2016; Dang et al., 2018). In the Gonghai Lake, the average concentration of
387 brGDGTs in SPM is 7.1 ± 2.0 ng/l in September and 5.2 ± 2.3 ng/l in January (Fig. 2) with no
388 significant difference. Besides, the compound IIIa", which is likely specifically of aquatic origin
389 (Weber et al., 2015), also showed no significant seasonal difference (0.36 ± 0.09 ng/l in September vs.
390 0.31 ± 0.15 ng/l in January). More importantly, the small differences in MBT'_{5ME} and MBT'_{6ME} of
391 SPM and their derived temperatures between September and January suggest that the actual seasonal
392 temperature difference, which may be recorded by the immediately produced brGDGTs, would have

393 been substantially masked or smoothed by the predominance of fossil brGDGTs. In addition,
394 brGDGT-derived temperatures in SPM were close to mean annual LWT and lower than the mean
395 warm season LWT, which also did not support the excessive production of brGDGTs during the
396 warm/summer season relative to winter season. Besides, the season of higher brGDGT concentration
397 has been found different in different lakes, e.g., in spring and autumn in Lower King Pond (Loomis et
398 al., 2014), in winter in Lake Lucerne (Blaga et al., 2011), and in summer in Lake Donghu in central
399 China (Qian et al., 2019). However, in all these lakes in temperate climate zones, the brGDGT-derived
400 temperatures have been found to be slightly or significantly warm season biased (Loomis et al., 2014;
401 Qian et al., 2019; Fig. 5b). The above evidence suggests that other factors, other than seasonality in
402 the production of brGDGTs in the lakes, should be responsible for the bias of brGDGT-inferred
403 temperature toward warm season in higher latitudes (Fig. 5b and c).

404 The brGDGT-derived temperature in lake sediments could be influenced by the vertically
405 inhomogeneous production of brGDGTs with maximum in deep/bottom waters. This seems true in the
406 Gonghai Lake as evidenced by the increase of sedimentary brGDGT content and the decrease of
407 brGDGT-derived temperature with water depth as discussed above. The bio-precursors of brGDGTs
408 have been proposed to be bacteria with an anaerobic heterotrophic lifestyle (Sinninghe Damsté et al.,
409 2000; Weijers et al., 2006b, 2010; Weber et al., 2015, 2018), implying that a potentially anoxic
410 (micro)environment in deep/bottom water favors the production of brGDGTs (Woltering et al., 2012;

411 Zhang et al., 2016; Weber et al., 2018). Such an occurrence could lead to higher proportion of ‘colder
412 temperature’ brGDGTs in lake sediments, which may at least partly interpret the frequently observed
413 cool bias of brGDGT-derived temperatures in many lakes, such as the Lake Challa, Lake Albert, Lake
414 Edward and Lake Tanganyika (Tierney et al., 2010; Loomis et al., 2012; Buckles et al., 2014a). The
415 MBT/CBT-derived temperature in the tropical Lake Huguangyan was thought to reflect mean annual
416 AT (Hu et al., 2015, 2016); however, has recently been proposed to be winter/cool biased (Chu et al.,
417 2017). We suppose that, as a monomictic lake, the lower mean annual temperature than mean annual
418 AT in deep/bottom waters might be a cause for the cool biased brGDGT temperature in the lake.
419 Intriguingly, all the above lakes are in the tropics. Nonetheless, the deep/bottom water bias may be
420 still true for the brGDGT-derived temperature in lakes in higher latitude, as suggested by our data in
421 the Gonghai Lake. However, different from those tropical lakes, in higher-latitude lakes, including the
422 Gonghai Lake (this study), Lake Qinghai (Wang et al., 2012), Lower King Pond (Loomis et al., 2014),
423 some cold-region lakes in China (Dang et al., 2018) and some Arctic lakes (Shanahan et al., 2013;
424 Peterse et al., 2014), the sedimentary brGDGT-derived temperatures are all higher, not lower, than the
425 mean annual AT. Therefore, more production of brGDGTs in deep/bottom water alone is not
426 responsible for the warm bias of brGDGT-derived temperature in surface sediments at least in these
427 lakes.

428 Although brGDGTs in lake sediments were confirmed to be mainly derived from in situ aquatic

429 production, previous studies deemed that the estimated temperatures can still reflect AT by assuming
430 that LWT is tightly coupled with AT (Tierney et al., 2010). In fact, such tight coupling can be found in
431 tropical-subtropical lakes, where AT is always above the freezing point, but is not true in
432 higher-latitude lakes such as Lower King Pond and Gonghai Lake with lake surface freezing in winter
433 (Fig. 6a and b). The reason is that lake surface ice prevents the thermal exchange between water and
434 air, leading to decoupling between LWT (usually ≥ 4 °C) and AT (< 0 °C) in winter in cold regions. The
435 decoupling makes mean annual LWT, even at the deep/bottom waters, higher than mean annual AT.
436 Therefore, the greater warm biases of brGDGT-derived temperatures from surface sediments in higher
437 latitudes (Fig. 5b) could be due to the stronger decoupling (e.g., longer freezing time) between LWT
438 and AT. Nevertheless, annual mean LWT appears basically close to the mean AT in warm season
439 (average monthly temperature > 0 °C) (Fig. 6f), which could be the reason why the brGDGT-inferred
440 temperatures are similar to the mean warm season AT (Fig. 5c). Due to lack of detailed AT and LWT
441 data in literature, we are hard to show more examples than as shown in Fig. 6, especially those from
442 even higher latitudes. However, we proposed a simple model for the relationship between LWT and
443 AT in a year cycle (Fig. 7), which may be a universal physical phenomenon in shallow lakes. In the
444 mid- and high-latitude region, we believe the decoupling between AT and LWT caused by ice
445 formation in winter may be applied to explain the observed seasonality of the brGDGT temperature
446 records. For example, the biases of brGDGT-derived temperatures toward summer AT observed

447 extensively in the Arctic and Antarctic lakes (Shanahan et al., 2013; Foster et al., 2016) are
448 compatible with the mechanism that we propose here. Of course, considering limited data in this study,
449 more investigations are needed to test our viewpoint in future studies.

450

451 **5 Conclusions**

452 We investigated the brGDGT distribution in catchment soils, surface sediments and water
453 column SPM in September and January in the Gonghai Lake in north China. The lake is characterized
454 by ice formation on its surface and a constant 4 °C condition in the underlying water in winter. The
455 brGDGT distribution in sediments were similar to that in SPM but differed clearly from that in soils,
456 indicating mainly in situ production of brGDGTs in the lake. BrGDGTs in SPM showed little seasonal
457 differences in concentration and MBT'_{5ME}, likely due to a dominant contribution of fossil brGDGTs
458 caused by, e.g., sediment suspension, which may mask any seasonal signals documented in
459 sedimentary brGDGTs. The increase of brGDGT content and decrease of methylation index with
460 water depth in sediments suggested more contribution of aquatic brGDGTs produced from
461 deep/bottom waters. Based on available lake calibrations, we found that the temperature estimates in
462 surface sediments and SPM of the Gonghai Lake were higher than the measured mean annual AT but
463 close to warm season AT, which cannot be interpreted by more aquatic production of brGDGTs in
464 warm season and/or in deep/bottom waters. We found that such a warm biased brGDGT-derived

465 temperature was actually close to the mean annual LWT, and therefore proposed that water-air
466 temperature decoupling due to ice formation at the lake surface in winter, which can prevent thermal
467 exchange between lake water and air, may be the cause for the apparent bias toward warm AT of
468 lacustrine brGDGT-derived temperatures. Since the warm AT bias of brGDGT estimates has been
469 observed extensively in mid- and high-latitude shallow lakes, we believe the mechanism proposed
470 here could also be applicable to these lakes.

471

472 **Data availability**

473 The raw data of this study can be accessed from <https://figshare.com/s/a4f324247ecd9d1ac575>.

474 **Author contribution**

475 ZR designed experiments, FS and JC collected samples and JC carried experiments out. JC, GJ and
476 ZR prepared the manuscript with contributions from all co-authors.

477 **Conflicts of interest**

478 The authors declare that they have no conflict of interest.

479

480 **Acknowledgments**

481 The work was supported by the Hunan Provincial Natural Science foundation of China (2018JJ1017),
482 the National Natural Science Foundation of China (41772373), and the Fundamental Research Funds

483 for the Central Universities of China (grant no. lzujbky-2018-it77). Two anonymous reviewers and
484 associate editor Marcel van der Meer are thanked for their valuable comments.

485

486 **References**

487 Ajioka, T., Yamamoto, M., and Murase, J.: Branched and isoprenoid glycerol dialkyl glycerol
488 tetraethers in soils and lake/river sediments in Lake Biwa basin and implications for MBT/CBT
489 proxies, *Org. Geochem.*, 73, 70-82, doi: 10.1016/j.orggeochem.2014.05.009, 2014.

490 Blaga, C. I., Reichart, G. J., Heiri, O., and Sinninghe Damsté, J. S.: Tetraether membrane lipid
491 distributions in water-column particulate matter and sediments: a study of 47 European lakes
492 along a north-south transect, *J. Paleolimnol.*, 41, 523-540, doi:10.1007/s10933-008-9242-2,
493 2009.

494 Blaga, C. I., Reichart, G. J., Schouten, S., Lotter, A. F., Werne, J. P., Kosten, S., Mazzeo, N., Lacerot,
495 G., and Sinninghe Damsté, J. S.: Branched glycerol dialkyl glycerol tetraethers in lake sediments:
496 can they be used as temperature and pH proxies, *Org. Geochem.*, 41, 1225-1234,
497 doi:10.1016/j.orggeochem.2010.07.002, 2010.

498 Blaga, C. I., Reichart, G. J., Vissers, E. W., Lotter, A. F., Anselmetti, F. S., and Sinninghe Damsté, J.
499 S.: Seasonal changes in glycerol dialkyl glycerol tetraether concentrations and fluxes in a
500 perialpine lake: Implications for the use of the TEX86 and BIT proxies, *Geochim. Cosmochim.*

501 Acta, 75, 6416-6428, doi:10.1016/j.gca.2011.08.016, 2011.

502 Buckles, L. K., Weijers, J. W. H., Verschuren, D., and Sinninghe Damsté, J. S.: Sources of core and
503 intact branched tetraether membrane lipids in the lacustrine environment: Anatomy of Lake
504 Challa and its catchment, equatorial East Africa, *Geochim. Cosmochim. Acta*, 140, 106-126,
505 doi:10.1016/j.gca.2014.04.042, 2014a.

506 Buckles, L. K., Weijers, J. W. H., Tran, X. M., Waldron, S., and Sinninghe Damsté, J. S.: Provenance
507 of tetraether membrane lipids in a large temperate lake (Loch Lomond, UK): implications for
508 glycerol dialkyl glycerol tetraether (GDGT)-based palaeothermometry, *Biogeosciences*, 11,
509 5539-5563, doi:10.5194/bg-11-5539-2014, 2014b.

510 Cao, J. T., Rao, Z. G., Jia, G. D., Xu, Q. H., and Chen, F. H.: A 15 ka pH record from an alpine lake in
511 north China derived from the cyclization ratio index of aquatic brGDGTs and its paleoclimatic
512 significance, *Org. Geochem.*, 109, 31-46, doi:10.1016/j.orggeochem.2017.02.005, 2017.

513 Chen, F. H., Yu, Z. C., Yang, M. L., Ito, E., Wang, S. M., Madsen, D. B., Huang, X. Z., Zhao, Y., Sato,
514 T., John, B. B. H., Boomer, I., Chen, J. H., An, C. B., and Wünnemann, B.: Holocene moisture
515 evolution in arid central Asia and its out-of-phase relationship with Asian monsoon history, *Quat.*
516 *Sci. Rev.*, 27, 351-364, doi:10.1016/j.quascirev.2007.10.017, 2008.

517 Chen, F. H., Liu, J. B., Xu, Q. H., Li, Y. C., Chen, J. H., Wei, H. T., Liu, Q. S., Wang, Z. L., Cao, X. Y.
518 and Zhang, S. R.: Environmental magnetic studies of sediment cores from Gonghai Lake:

519 implications for monsoon evolution in North China during the late glacial and Holocene, J.
520 Paleolimnol., 49, 447-464, doi:10.1007/s10933-012-9677-3, 2013.

521 Chen, F. H., Xu, Q. H., Chen, J. H., Birks, H. J. B., Liu, J. B., Zhang, S. R., Jin, L. Y., An, C. B.,
522 Telford, R. J., Cao, X. Y., Wang, Z. L., Zhang, X. J., Selvaraj, K., Lu, H. Y., Li, Y. C., Zheng, Z.,
523 Wang, H. P., Zhou, A. F., Dong, G. H., Zhang, J. W., Huang, X. Z., Bloemendal, J. and Rao, Z.
524 G.: East Asian summer monsoon precipitation variability since the last deglaciation, Sci. Rep., 5,
525 11186, doi:10.1038/srep11186, 2015.

526 Chu, G., Sun, Q., Zhu, Q., Shan, Y., Shang, W., Ling, Y., Su, Y., Xie, M., Wang, X., Liu, J.: The role
527 of the Asian winter monsoon in the rapid propagation of abrupt climate changes during the last
528 deglaciation, Quat. Sci. Rev., 177, 120-129, doi:10.1016/j.quascirev.2017.10.014, 2017.

529 Dang, X. Y., Ding, W. H., Yang, H., Pancost, R. D., Naafs, B. D. A., Xue, J. T., Lin, X., Lu, J. Y., and
530 Xie, S. C.: Different temperature dependence of the bacterial brGDGT isomers in 35 Chinese
531 lake sediments compared to that in soils, Org. Geochem., 119, 72-79,
532 doi:10.1016/j.orggeochem.2018.02.008, 2018.

533 De Jonge, C., Hopmans, E.C., Stadnitskaia, A., Rijpstra, W. I. C., Hofland, R., Tegelaar, E., Sinninghe
534 Damsté, J. S.: Identification of novel penta- and hexamethylated branched glycerol dialkyl
535 glycerol tetraethers in peat using HPLC-MS², GC-MS and GC-SMB-MS, Org. Geochem., 54,
536 78-82, doi:10.1016/j.orggeochem.2012.10.004, 2013.

- 537 De Jonge, C., Hopmans, E. C., Zell, C. I., Kim, J. H., Schouten, S., and Sinninghe Damsté, J. S.:
538 Occurrence and abundance of 6-methyl branched glycerol dialkyl glycerol tetraethers in soils:
539 implications for palaeoclimate reconstruction, *Geochim. Cosmochim. Acta*, 141, 97-112,
540 doi:10.1016/j.gca.2014.06.013, 2014.
- 541 De Jonge, C., Radujković, D., Sigurdsson, B. D., Weedon, J. T., Janssens, I., Peterse, F.: Lipid
542 biomarker temperature proxy responds to abrupt shift in the bacterial community composition in
543 geothermally heated soils, *Org. Geochem.*, 137, 103897, doi:10.1016/j.orggeochem.2019.07.006,
544 2019.
- 545 Deng, L. H., Jia, G. D., Jin, C. F., and Li, S. J.: Warm season bias of branched GDGT temperature
546 estimates causes underestimation of altitudinal lapse rate, *Org. Geochem.*, 96, 11-17,
547 doi:10.1016/j.orggeochem.2016.03.004, 2016.
- 548 Foster, L. C., Pearson, E. J., Juggins, S., Hodgson, D. A., Saunders, K. M., Verleyen, E., and Roberts,
549 S. J.: Development of a regional glycerol dialkyl glycerol tetraether (GDGT)-temperature
550 calibration for Antarctic and sub-Antarctic lakes, *Earth Planet. Sci. Lett.*, 433, 370-379,
551 doi:10.1016/j.epsl.2015.11.018, 2016.
- 552 Hopmans, E. C., Weijers, J. W. H., Schefuß, E., Herfort, L., Sinninghe Damsté, J. S., and Schouten, S.:
553 A novel proxy for terrestrial organic matter in sediments based on branched and isoprenoid
554 tetraether lipids, *Earth Planet. Sci. Lett.*, 224, 107-116, doi:10.1016/j.epsl.2004.05.012, 2004.

555 Hu, J. F., Zhou, H. D., Peng, P. A., Yang, X. P., Spiro, B., Jia, G. D., Wei, G. J. and Ouyang, T. P.:
556 Reconstruction of a paleotemperature record from 0.3-3.7 ka for subtropical South China using
557 lacustrine branched GDGTs from Huguangyan Maar, *Paleogeogr. Paleoclimatol. Paleoecol.*, 435,
558 167-176, doi:10.1016/j.palaeo.2015.06.014, 2015.

559 Hu, J. F., Zhou, H. D., Peng, P. A., and Spiro, B.: Seasonal variability in concentrations and fluxes of
560 glycerol dialkyl glycerol tetraethers in Huguangyan Maar Lake, SE China: Implications for the
561 applicability of the MBT-CBT paleotemperature proxy in lacustrine settings, *Chem. Geol.*, 420,
562 200-212, doi:10.1016/j.chemgeo.2015.11.008, 2016.

563 Huguet, C., Hopmans, E. C., Febo-Ayala, W., Thompson, D. H., Sinninghe Damsté, J. S., and
564 Schouten, S.: An improved method to determine the absolute abundance of glycerol dibiphytanyl
565 glycerol tetraether lipids, *Org. Geochem.*, 37, 1036-1041,
566 doi:10.1016/j.orggeochem.2006.05.008, 2006.

567 Loomis, S. E., Russell, J. M., and Sinninghe Damsté, J. S.: Distributions of branched GDGTs in soils
568 and lake sediments from western Uganda: implications for a lacustrine paleothermometer, *Org.*
569 *Geochem.*, 42, 739-751, doi:10.1016/j.orggeochem.2011.06.004, 2011.

570 Loomis, S. E., Russell, J. M., Ladd, B., Street-Perrott, F. A., and Sinninghe Damsté, J. S.: Calibration
571 and application of the branched GDGT temperature proxy on East African lake sediments, *Earth*
572 *Planet. Sci. Lett.*, 357-358, 277-288, doi:10.1016/j.epsl.2012.09.031, 2012.

573 Loomis, S. E., Russell, J. M., Heureux, A. M., Andrea, W. J. D., and Sinninghe Damsté, J. S.:
574 Seasonal variability of branched glycerol dialkyl glycerol tetraethers (brGDGTs) in a temperate
575 lake system, *Geochim. Cosmochim. Acta*, 144, 173-187, doi:10.1016/j.gca.2014.08.027, 2014.

576 Lu, H. X., Liu, W. G., Yang, H., Wang, H. Y., Liu, Z. H., Leng, Q., Sun, Y. B., Zhou, W. J., and An, Z.
577 S.: 800-kyr land temperature variations modulated by vegetation changes on Chinese Loess
578 Plateau, *Nat. Commun.*, 10, 1958, doi:10.1038/s41467-019-09978-1, 2019.

579 Martin, C., Ménot, G., Thouveny, N., Davtian, N., Andrieu-Ponel, V., Reille, M., and Bard, E.: Impact
580 of human activities and vegetation changes on the tetraether sources in Lake St Front (Massif
581 Central, France), *Org. Geochem.*, 135, 38–52, doi:10.1016/j.orggeochem.2019.06.005, 2019.

582 Naeher, S., Peterse, F., Smittenberg, R. H., Niemann, H., Zigah, P. K., and Schubert, C. J.: Sources of
583 glycerol dialkyl glycerol tetraethers (GDGTs) in catchment soils, water column and sediments of
584 Lake Rotsee (Switzerland)-implications for the application of GDGT-based proxies for lakes,
585 *Org. Geochem.*, 66, 164-173, doi:10.1016/j.orggeochem.2013.10.017, 2014.

586 Naafs, B. D. A., Gallego-Sala, A. V., Inglis, G. N., and Pancost, R. D.: Refining the global branched
587 glycerol dialkyl glycerol tetraether (brGDGT) soil temperature calibration, *Org. Geochem.*, 106,
588 48-56, doi:10.1016/j.orggeochem.2017.01.009, 2017.

589 Niemann, H., Stadnitskaia, A., Wirth, S. B., Gilli, A., Anselmetti, F. S., Sinninghe Damsté, J. S.,
590 Schouten, S., Hopmans, E. C., and Lehmann, M. F.: Bacterial GDGTs in Holocene sediments

591 and catchment soils of a high Alpine lake: application of the MBT/CBT-paleothermometer, *Clim.*
592 *Past*, 8, 889-906, doi: 10.5194/cp-8-889-2012, 2012.

593 Pearson, E. J., Juggins, S., Talbot, H. M., Weckström, Jan., Rosén, P., Ryves, D. B., Roberts, S. J., and
594 Schmidt, R.: A lacustrine GDGT-temperature calibration from the Scandinavian Arctic to
595 Antarctic: renewed potential for the application of GDGT-paleothermometry in lakes, *Geochim.*
596 *Cosmochim. Acta*, 75, 6225-6238, doi: 10.1016/j.gca.2011.07.042, 2011.

597 Peterse, F., van der Meer, J., Schouten, S., Weijers, J. W. H., Fierer, N., Jackson, R. B., Kim, J. M.,
598 and Sinninghe Damsté, J. S.: Revised calibration of the MBT-CBT paleotemperature proxy based
599 on branched tetraether membrane lipids in surface soils, *Geochim. Cosmochim. Acta*, 96,
600 215-229, doi:10.1016/j.gca.2012.08.011, 2012.

601 Peterse, F., Vonk, J. E., Holmes, R. M., Giosan, L., Zimov, N., and Eglinton, T. I.: Branched glycerol
602 dialkyl glycerol tetraethers in Arctic lake sediments: sources and implications for
603 paleothermometry at high latitudes, *J. Geophys. Res.-Biogeosci.*, 119, 1738-1754, doi:
604 10.1002/2014jg002639, 2014.

605 Qian, S., Yang, H., Dong, C. H., Wang, Y. B., Wu, J., Pei, H. Y., Dang, X. Y., Lu, J. Y., Zhao, S. J., and
606 Xie, S. C.: Rapid response of fossil tetraether lipids in lake sediments to seasonal environmental
607 variables in a shallow lake in central China: Implications for the use of tetraether-based proxies,
608 *Org. Geochem.*, 128, 108-121, doi:10.1016/j.orggeochem.2018.12.007, 2019.

- 609 Rao, Z. G., Jia, G. D., Li, Y. X., Chen, J. H., Xu, Q. H., and Chen, F. H.: Asynchronous evolution of
610 the isotopic composition and amount of precipitation in north China during the Holocene
611 revealed by a record of compound-specific carbon and hydrogen isotopes of long-chain
612 *n*-alkanes from an alpine lake, *Earth Planet. Sci. Lett.*, 446, 68-76,
613 doi:10.1016/j.epsl.2016.04.027, 2016.
- 614 Russell, J. M., Hopmans, E. C., Loomis, S. E., Liang, J., and Sinninghe Damsté, J. S.: Distributions of
615 5- and 6-methyl branched glycerol dialkyl glycerol tetraethers (brGDGTs) in East African lake
616 sediment: Effects of temperature, pH, and new lacustrine paleotemperature calibrations, *Org.*
617 *Geochem.*, 117, 56-69, doi:10.1016/j.orggeochem.2017.12.003, 2018.
- 618 Schoon, P. L., de Kluijver, A., Middelburg, J. J., Downing, J. A., Sinninghe Damsté, J. S., and
619 Schouten, S.: Influence of lake water pH and alkalinity on the distribution of core and intact
620 polar branched glycerol dialkyl glycerol tetraethers (GDGTs) in lakes, *Org. Geochem.*, 60, 72-82,
621 doi:10.1016/j.orggeochem.2013.04.015, 2013.
- 622 Schouten, S., Hopmans, E. C., and Sinninghe Damsté, J. S.: The organic geochemistry of glycerol
623 dialkyl glycerol tetraether lipids: a review, *Org. Geochem.*, 54, 19-61,
624 doi:10.1016/j.orggeochem.2012.09.006, 2013.
- 625 Shanahan, T. M., Hughen, K. A., and Van Mooy, B. A. S.: Temperature sensitivity of branched and
626 isoprenoid GDGTs in Arctic lakes, *Org. Geochem.*, 64, 119-128,

627 doi:10.1016/j.orggeochem.2013.09.010, 2013.

628 Shen, Z. W., Liu, J. B., Xie, C. L., Zhang, X. S., and Chen, F. H.: An environmental perturbation at
629 AD 600 and subsequent human impacts recorded by multi-proxy records from the sediments of
630 Lake Mayinghai, North China, *The Holocene*, 28, 1870-1880, doi: 10.1177/0959683618798159,
631 2018.

632 Sinninghe Damsté, J. S., Hopmans, E. C., and Pancost, R. D.: Newly discovered non-isoprenoid
633 glycerol dialkyl glycerol tetraether lipids in sediments, *Chem. Commun.*, 23, 1683-1684, doi:
634 10.1039/b004517i, 2000.

635 Sinninghe Damsté, J. S.: Spatial heterogeneity of sources of branched tetraethers in shelf systems: The
636 geochemistry of tetraethers in the Berau River delta (Kalimantan, Indonesia), *Geochim.
637 Cosmochim. Acta*, 186, 13-31, doi:10.1016/j.gca.2016.04.033, 2016.

638 Sun, Q., Chu, G. Q., Liu, M. M., Xie, M. M., Li, S. Q., Ling, Y., Wang, X. H., Shi, L. M., Jia, G. D.,
639 and Lü, H. Y.: Distributions and temperature dependence of branched glycerol dialkyl glycerol
640 tetraethers in recent lacustrine sediments from China and Nepal, *J. Geophys. Res.*, 116, G01008,
641 doi: 10.1029/2010jg001365, 2011.

642 Tierney, J. E., and Russell, J. M.: Distributions of branched GDGTs in a tropical lake system:
643 implications for lacustrine application of the MBT/CBT paleoproxy, *Org. Geochem.*, 40,
644 1032-1036, doi:10.1016/j.orggeochem.2009.04.014, 2009.

- 645 Tierney, J. E., Russell, J. M., Eggermont, H., Hopmans, E. C., Verschuren, D., and Sinninghe Damsté,
646 J. S.: Environmental controls on branched tetraether lipid distributions in tropical East African
647 lake sediments, *Geochim. Cosmochim. Acta*, 74, 4902-4918, doi:10.1016/j.gca.2010.06.002,
648 2010.
- 649 Tierney, J. E., Schouten, S., Pitcher, A., Hopmans, E. C., and Sinninghe Damsté, J. S.: Core and intact
650 polar glycerol dialkyl glycerol tetraethers (GDGTs) in Sand Pond, Warwick, Rhode Island (USA):
651 insights into the origin of lacustrine GDGTs, *Geochim. Cosmochim. Acta*, 77, 561-581, doi:
652 10.1016/j.gca.2011.10.018, 2012.
- 653 Wang, H. Y., Liu, W. G., Zhang, C. L., Wang, Z., Wang, J. X., Liu, Z. H., and Dong, H. L.:
654 Distribution of glycerol dialkyl glycerol tetraethers in surface sediments of Lake Qinghai and
655 surrounding soil, *Org. Geochem.*, 47, 78-87, doi:10.1016/j.orggeochem.2012.03.008, 2012.
- 656 Wang, H. Y., Liu, W. G., Lu, H. X.: Appraisal of branched glycerol dialkyl glycerol tetraether-based
657 indices for North China, *Org. Geochem.*, 98, 118-130, doi:10.1016/j.orggeochem.2016.05.013,
658 2016.
- 659 Wang, M. Y., Zheng, Z., Zong, Y. Q., Tian, L. P.: Distributions of soil branched glycerol dialkyl
660 glycerol tetraethers from different climate regions of China, *Sci Rep.*, 9, 2761, doi:
661 10.1038/s41598-019-39147-9, 2019.
- 662 Weber, Y., De Jonge, C., Rijpstra, W. I. C., Hopmans, E. C., Stadnitskaia, A., Schubert, C. J.,

663 Lehmann, M. F., Sinninghe Damsté, J. S., and Niemann, H.: Identification and carbon isotope
664 composition of a novel branched GDGT isomer in lake sediments: evidence for lacustrine
665 branched GDGT production, *Geochim. Cosmochim. Acta*, 154, 118-129,
666 doi:10.1016/j.gca.2015.01.032, 2015.

667 Weber, Y., Sinninghe Damsté, J. S., Zopfi, J., De Jonge, C., Gilli, A., Schubert, C. J., Lepori, F.,
668 Lehmann, M. F., and Niemann, H.: Redox-dependent niche differentiation provides evidence for
669 multiple bacterial sources of glycerol tetraether lipids in lakes, *Proc. Natl. Acad. Sci. USA*, 115,
670 10926-10931, doi:10.1073/pnas.1805186115, 2018.

671 Weijers, J. W. H., Schouten, S., Spaargaren, O. C., and Sinninghe Damsté, J. S.: Occurrence and
672 distribution of tetraether membrane lipids in soils: Implications for the use of the TEX86 proxy
673 and the BIT index, *Org. Geochem.*, 37, 1680-1693, doi:10.1016/j.orggeochem.2006.07.018,
674 2006a.

675 Weijers, J. W. H., Schouten, S., Hopmans, E. C., Geenevasen, J. A. J., David, O. R. P., Coleman, J. M.,
676 Pancost, R. D., and Sinninghe Damsté, J. S.: Membrane lipids of mesophilic anaerobic bacteria
677 thriving in peats have typical archaeal traits, *Environ. Microbiol.*, 8, 648-657,
678 doi:10.1111/j.1462-2920.2005.00941.x, 2006b.

679 Weijers, J. W. H., Schouten, S., Van den Donker, J. C., Hopmans, E. C., and Sinninghe Damsté, J. S.:
680 Environmental controls on bacterial tetraether membrane lipid distribution in soils, *Geochim.*

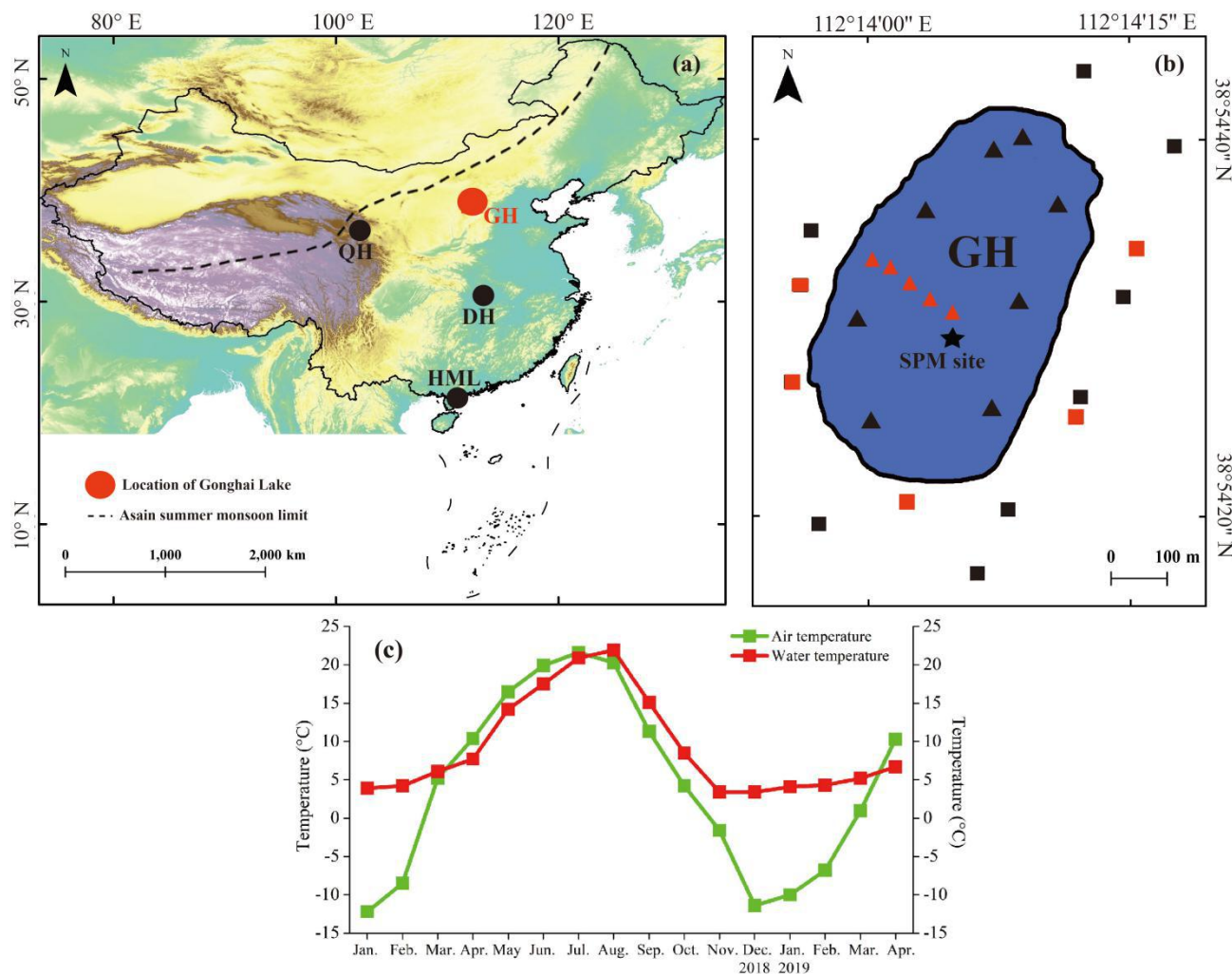
- 681 Cosmochim. Acta, 71, 703-713, doi:10.1016/j.gca.2006.10.003, 2007a.
- 682 Weijers, J. W. H., Schefuß, N., Schouten, S., and Sinninghe Damsté, J. S.: Coupled thermal and
683 hydrological evolution of tropical Africa over the last deglaciation, *Science*, 315, 1701-1704,
684 doi:10.1126/science.1138131, 2007b.
- 685 Weijers, J. W. H., Wiesenberg, G. L. B., Bol, R., Hopmans, E. C., and Pancost, R. D.: Carbon isotopic
686 composition of branched tetraether membrane lipids in soils suggest a rapid turnover and a
687 heterotrophic life style of their source organism(s), *Biogeosciences*, 7, 2959-2973, doi:
688 10.5194/bgd-7-3691-2010, 2010.
- 689 Woltering, M., Werne, J. P., Kish, J. L., Hicks, R., Sinninghe Damsté, J. S., Schouten, S.: Vertical and
690 temporal variability in concentration and distribution of thaumarchaeotal tetraether lipids in Lake
691 Superior and the implications for the application of the TEX86 temperature proxy, *Geochim.
692 Cosmochim. Acta*, 87, 136-153, doi:10.1016/j.gca.2012.03.024, 2012.
- 693 Xiao, W. J., Wang, Y. H., Zhou, S. Z., Hu, L. M., Yang, H., Xu, Y. P.: Ubiquitous production of
694 branched glycerol dialkyl glycerol tetraethers (brGDGTs) in global marine environments: a new
695 source indicator for brGDGTs, *Biogeosciences*, 13, 5883–5894, doi:10.5194/bg-13-5883-2016,
696 2016.
- 697 Yang, H., Lü, X. X., Ding, W. H., Lei, Y. Y., Dang, X. Y., Xie, S. C.: The 6-methyl branched
698 tetraethers significantly affect the performance of the methylation index (MBT') in soils from an

699 altitudinal transect at Mount Shennongjia, *Org. Geochem.*, 82, 42–53,
700 doi:10.1016/j.orggeochem.2015.02.003, 2015.

701 Zhang, J., Yu, Z. G., Jia, G. D.: Cyclisation degree of tetramethylated brGDGTs in marine
702 environments and its implication for source identification, *Global Planet. Change*, 184, 103043,
703 doi:10.1016/j.gloplacha.2019.103043, 2020.

704 Zhang, Z. H., Smittenberg, R. H., and Bradley, R. S.: GDGT distribution in a stratified lake and
705 implications for the application of TEX86 in paleoenvironmental reconstructions, *Sci. Rep.*, 6,
706 34465, doi:10.1038/srep34465, 2016.

707 **Captions for Tables and Figures:**



708

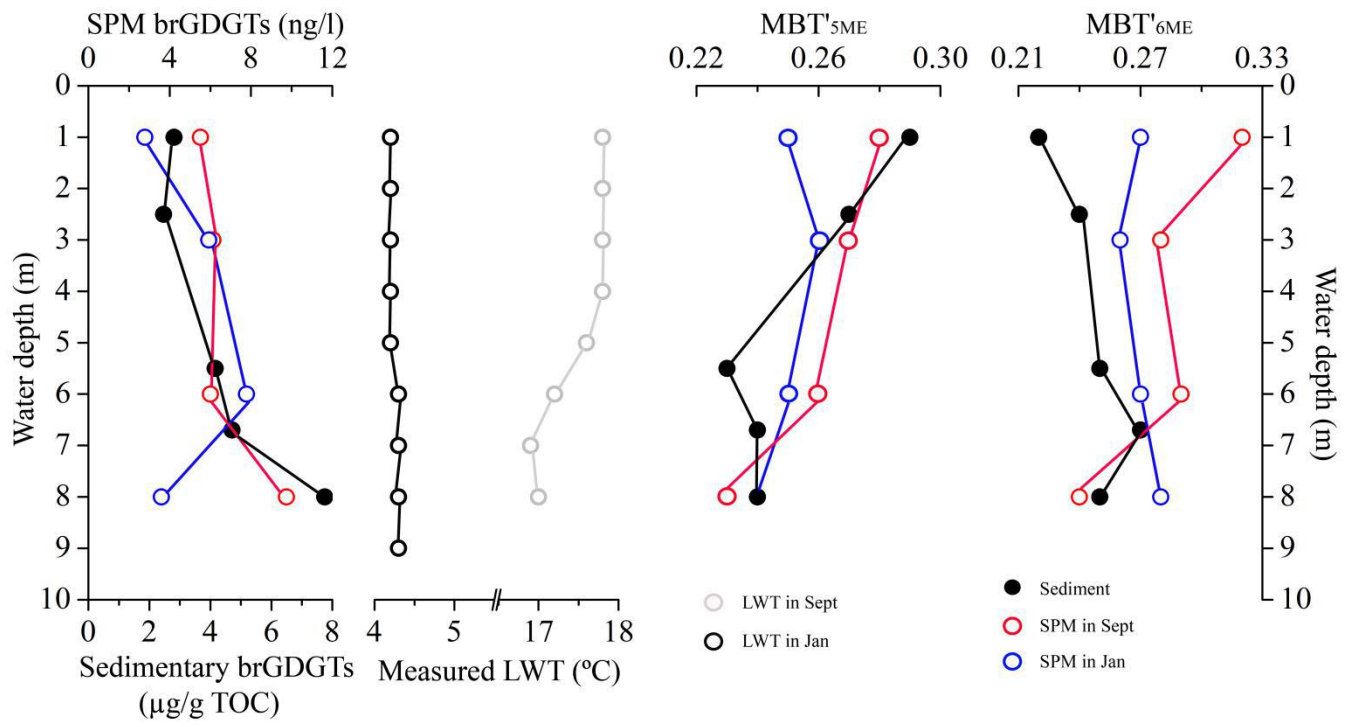
709 **Fig. 1.** (a) The Gonghai Lake (red circle), other referenced lakes (black circles) and modern Asian summer monsoon

710 limit (dashed line; Chen et al., 2008). (b) SPM from water column (black star), surface soils (red squares) and

711 surface sediments (red triangles) in Gonghai Lake in this study; black squares and triangles represents the

712 sample sites published in Cao et al. (2017) (modified from Cao et al., 2017). (c) Measured local air temperature

713 (AT) and lake water temperature (LWT) during 2018–2019 (this study).

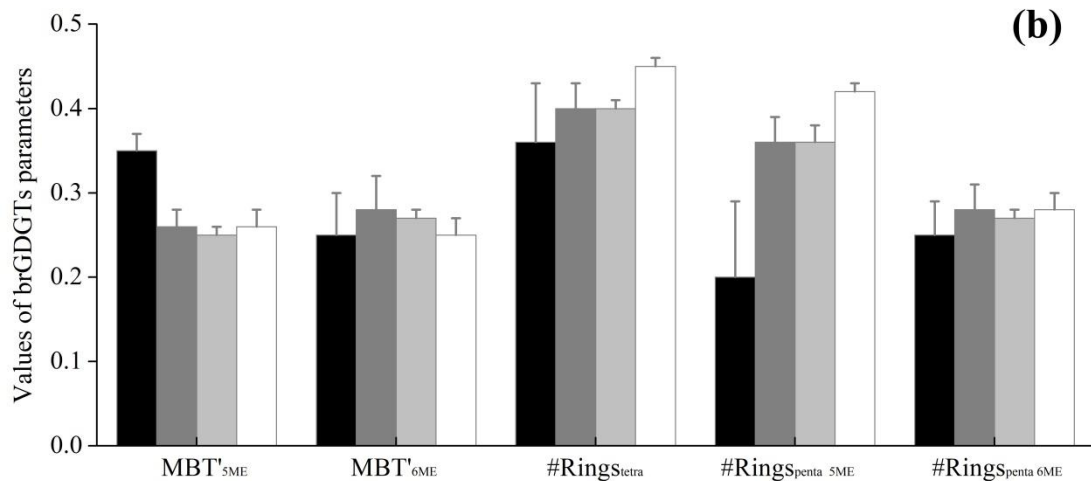
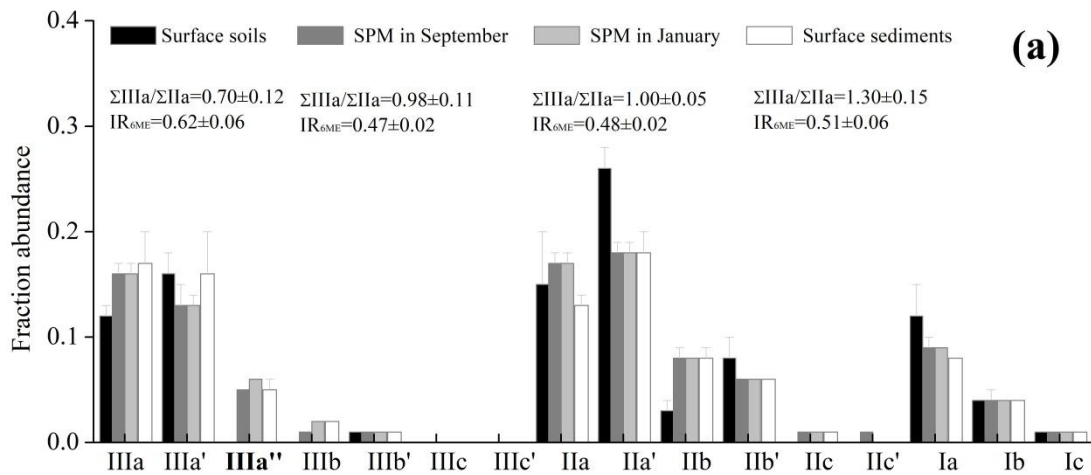


714

715 **Fig. 2.** Depth profiles of water temperature, brGDGT concentrations, MBT'_{5ME}, MBT'_{6ME} in water SPM from

716 January and September and sediments in the Gonghai Lake.

717

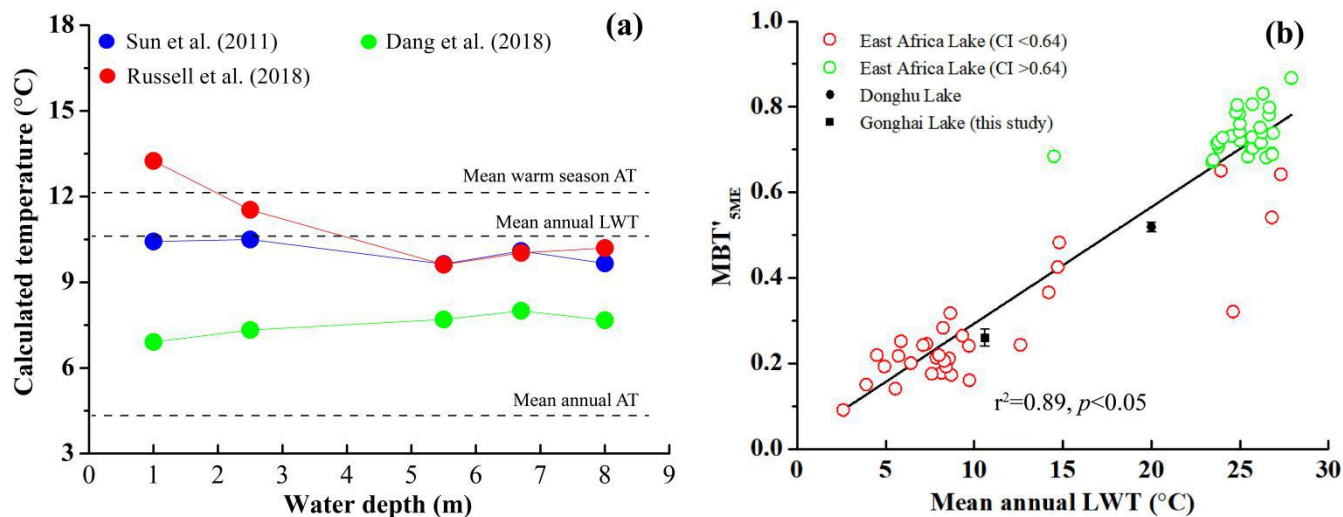


718

719 **Fig. 3.** BrGDGT distribution in surface soils, water column (SPM) and surface sediments of the Gonghai Lake. (a)

720 Fractional abundance of brGDGTs. (b) Degree of methylation and cyclisation of brGDGTs.

721



722

723 **Fig. 4.** (a) BrGDGT-derived temperatures for sediments using lake calibrations Eqs. (11), (15) and (16) from Sun et

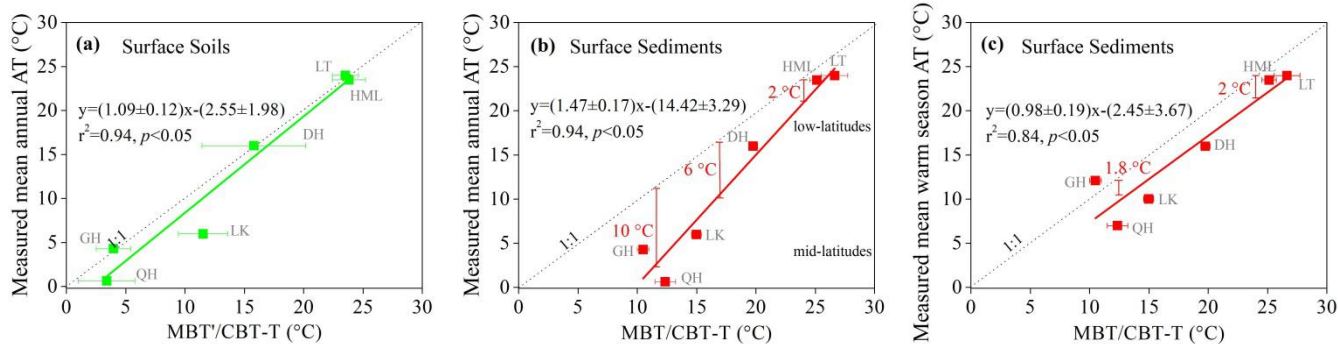
724 al. (2011), Dang et al. (2018) and Russell et al. (2018) respectively. (b) The correlation between MBT'_{5ME} of

725 sedimentary brGDGTs and mean annual lake water temperature (LWT); CI index represents Community Index

726 (De Jonge et al., 2019); the brGDGT data of East Africa Lake, Lake Donghu and Gonghai Lake were sourced

727 from Russell et al. (2018), Qian et al. (2019) and this study.

728



729

730 **Fig. 5.** Comparison of brGDGT-derived temperature and measured air temperature. (a) Measured mean AT

731 and estimated temperatures of brGDGTs in surface soils based on soil calibration Eq. (9). (b) Measured mean

732 annual AT and estimated temperatures of brGDGTs in surface sediments based on lake calibration Eq. (11). (c)

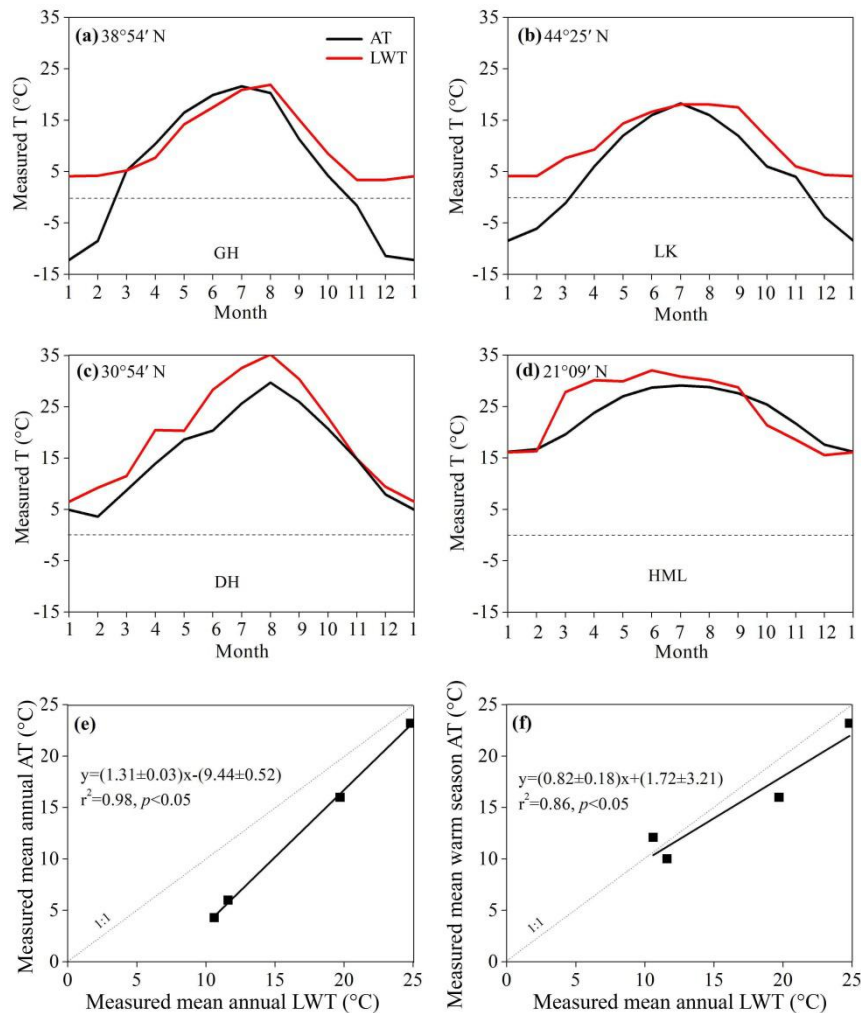
733 Measured mean warm season AT and estimated temperatures of brGDGTs in surface sediments based on lake

734 calibration Eq. (11). Data are from Gonghai Lake (GH; Cao et al., 2017), Lower King Pond (LK; Loomis et al.,

735 2014), Lake Huguangyan (HML; Hu et al., 2015, 2016), Lake Donghu (DH; Qian et al., 2019), Lake Qinghai

736 (QH; Wang et al., 2012) and Lake Towuli (LT; Tierney and Russell, 2009).

737



738

739 **Fig. 6.** Measured LWT and AT in (a) Gonghai Lake (GH; this study), (b) Lower King Pond (LK; modified from

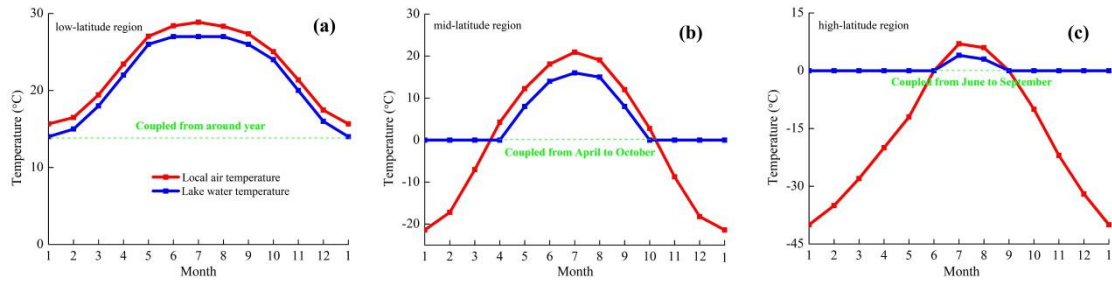
740 Loomis et al., 2014), (c) Lake Donghu (DH; modified from Qian et al., 2019) and (d) Lake Huguangyan (HML;

741 modified from Hu et al., 2016). (e) Correlation between mean annual AT and mean annual LWT. (f) Correlation

742 between mean warm season AT and mean annual LWT. In the mid-latitude Gonghai Lake and Lower King

743 Pond, the surface LWT follows AT only when the AT is above freezing. In the low-latitude Lake Donghu and

744 Lake Huguangyan, the surface LWT follows AT for the whole year.



745

746

Fig. 7. A simple model showing the relationship between LWT and AT in an annual cycle in different latitudes.

Table 1 Concentration of brGDGTs, MBT'_{5ME}, MBT'_{6ME} and estimated temperatures in catchment surface soils, sediments and water column SPM in the Gonghai Lake.

Code of site	Longitude (E)	Latitude (N)	Vegetation type	Water depth (m)	IIIa' (ng/g dw) (ng/L)	Total brGDGTs		MAAT ^a (° C)	MAAT ^b (° C)	MAAT ^c (° C)	MAAT ^d (° C)	Growth AT ^e (° C)	
						MBT' _{5ME}	MBT' _{6ME}						
Surface soils in Gonghai catchment													
S1	112° 14'19.039"	38° 54'37.343"	grass		0	74.82	0.31	0.21	1.20	-2.90			
S2	112° 14'18.460"	38° 54'28.750"	grass		0	23.50	0.36	0.20	2.58	-1.21			
S3	112° 14'24.140"	38° 54'23.098"	shrub		0	22.00	0.35	0.33	2.40	-4.22			
S4	112° 14'36.827"	38° 54'27.126"	shrub		0	32.65	0.36	0.26	2.64	-2.15			
S5	112° 14'40.502"	38° 54'38.174"	grass		0	16.06	0.36	0.24	2.82	-1.61			
Gonghai surface sediments													
D1	112° 14'22.963"	38° 54'36.357"		1.00	1.46	42.03	0.29	0.22	0.70	-4.24	8.35	13.50	6.91
D2	112° 14'24.004"	38° 54'35.903"		2.50	1.59	33.95	0.27	0.24	-0.13	-4.79	7.50	11.91	7.33
D3	112° 14'25.109"	38° 54'35.294"		5.50	17.87	327.62	0.23	0.25	-1.19	-6.53	6.40	10.11	7.70
D4	112° 14'27.301"	38° 54'34.499"		6.70	25.53	374.29	0.24	0.27	-0.93	-7.32	6.67	10.57	8.00
D5	112° 14'28.453"	38° 54'33.980"		8.00	42.96	706.72	0.24	0.25	-0.95	-6.44	6.64	10.72	7.67
Gonghai SPM in Sept													
Water-1 m	112° 14'28.453"	38° 54'33.980"		1.00	0.29	5.71	0.28	0.32	0.24	-6.00	7.88	11.19	9.16
Water-3 m	112° 14'28.453"	38° 54'33.980"		3.00	0.36	6.39	0.27	0.28	-0.05	-5.46	7.57	10.86	8.25
Water-6 m	112° 14'28.453"	38° 54'33.980"		6.00	0.30	6.22	0.26	0.29	-0.35	-6.55	7.26	10.45	8.55
Water-8 m	112° 14'28.453"	38° 54'33.980"		8.00	0.49	10.07	0.23	0.24	-1.40	-6.79	6.18	10.60	7.31
Gonghai SPM in Jan													
Water-1 m	112° 14'28.453"	38° 54'33.980"		1.00	0.16	2.88	0.25	0.27	-0.75	-6.32	6.85	10.40	7.95
Water-3 m	112° 14'28.453"	38° 54'33.980"		3.00	0.36	6.09	0.26	0.26	-0.49	-5.57	7.12	11.02	7.77
Water-6 m	112° 14'28.453"	38° 54'33.980"		6.00	0.49	8.05	0.25	0.27	-0.65	-6.24	6.95	10.57	7.99
Water-8 m	112° 14'28.453"	38° 54'33.980"		8.00	0.22	3.71	0.24	0.28	-0.96	-6.89	6.63	10.20	8.24

MAAT represents mean annual air temperature.

^a Calculated according to Eq. (9).

^b Calculated according to Eq. (10).

^c and ^d Calculated according to Eq. (16) and (17).

^e Calculated according to Eq. (15).

750

Table 2 Calibrations for brGDGT-derived temperature proxies used in this study.

Calibrations	Equation no. in the text	References
For soils		
MAAT=0.81-5.67*CBT+31.0*MBT ^a (<i>n</i> =176, <i>r</i> ² =0.59, RMSE=5.0 ° C)	(8)	Peterse et al. (2012)
MAAT=-8.57+31.45*MBT ^a _{SME} (<i>n</i> =222, <i>r</i> ² =0.66, RMSE=4.8 ° C)	(9)	De Jonge et al. (2014)
MAAT ^a =27.63*Index 1-5.72 (<i>n</i> =148, <i>r</i> ² =0.75, RMSE=2.5 ° C)	(10)	Wang et al. (2016)
For sediments		
MAAT=6.803-7.062*CBT+37.09*MBT (<i>n</i> =139, <i>r</i> ² =0.62, RMSE=5.24 ° C)	(11)	Global, Sun et al. (2011)
MAAT=8.263-17.938*CBT+46.675*MBT (<i>n</i> =24, <i>r</i> ² =0.52, RMSE=5.1 ° C)	(12)	Regional, Sun et al. (2011)
MAAT ^b =50.47-74.18*f(IIIa)-31.60*f(IIa)-34.69*f(Ia) (<i>n</i> =46, <i>r</i> ² =0.94, RMSE=2.2 ° C)	(13)	Tierney et al. (2010)
MAAT=22.77-33.58*f(IIIa)-12.88*f(IIa)-418.53*f(IIc)+86.43*f(Ib) (<i>n</i> =111, <i>r</i> ² =0.94, RMSE=1.9 ° C)	(14)	Loomis et al. (2012)
Growth AT=21.39*MBT ^a _{6ME} +2.27 (<i>n</i> =39, <i>r</i> ² =0.75, RMSE=1.78 ° C)	(15)	Dang et al. (2018)
MAAT=23.81-31.02*f(IIIa)-41.91*f(IIb)-51.59*f(IIb')-24.70*f(IIa)+68.80*f(Ib) (<i>n</i> =65, <i>r</i> ² =0.94, RMSE=2.14 ° C)	(16)	Russell et al. (2018)
MAAT=-1.21+32.42*MBT ^a _{SME}	(17)	Russell et al. (2018)

755 AT represents air temperature.

MAAT represents mean annual air temperature.

^a Index=log[(Ia+Ib+Ic+IIa'+IIIa')/(Ic+IIa+IIc+IIIa+IIIa')].

^b Fractional abundance of brGDGTs is a fraction of only brGDGT Ia, IIa and IIIa.

Table 3 Comparison of measured air temperature, brGDGT-derived temperature from catchment soils and

brGDGT-derived temperature from sediments in different lake basins.

Name	Latitude	Longitude	Depth (m)	MAA T (° C)	Mean warm season AT (° C)	Mean annual LWT (° C)	Surface					References
							soils		Surface sediments			
							MAAT ^a (° C)	MAAT ^b (° C)	MAAT ^c (° C)	MAAT ^d (° C)	MAAT ^e (° C)	
Gonghai Lake	38° 54' N	112° 14' E	9	4.3	12.1	10.6	3.96±1.46	10.74±0.33	9.70±0.71	10.86±1.33	7.93±1.46	Cao et al. (2017)
Lake Towuti	2.5° S	121° E	200	24	24	n.d.	22.52±2.61	26.62±1.10	29.13±1.86	n.d.	n.d.	Tierney and Russell. (2009)
Lake Huguanyan	21° 09' N	110° 17' E	20	23.2	23.2	24.8	23.80±1.39	25.11±0.60	28.12±0.90	26.47±0.83	26.07±0.73	Hu et al. (2015, 2016)
Lake Donghu	30° 54' N	114° 41' E	6	16	16	20	15.79±4.37	19.74±0.39	22.82±0.51	25.75±0.34	20.61±0.71	Qian et al. (2019)
Lake Qinghai	36° 54' N	100° 01' E	27	0.65	7	n.d.	3.38±2.40	12.34±0.87	9.92±1.14	13.61±1.49	8.80±1.11	Wang et al. (2012)
Lower King Pond	44° 25' N	72° 26' W	8	6	11.3	11.6	11.50±2.08	14.97±0.42	14.9±0.53	18.75±0.64	15.76±0.84	Loomis et al. (2014)

AT represents air temperature and MAAT represents mean annual air temperature.

LWT represents lake water temperature.

^a Calculated according to Eq. (8).

^b and ^c Calculated according to Eq. (11) and (12).

^d Calculated according to Eq. (13).

^e Calculated according to Eq. (14).

760

765